

Discovering the Gell-Mann–Okubo Formula with Kolmogorov–Arnold Networks

Jian-Yao He,¹ Xun Chen,^{1,2,*} Xiao-Yan Zhu,^{3,†} and Wen Luo^{1,‡}

¹*School of Nuclear Science and Technology, University of South China Hengyang, No 28, West Changsheng Road, Hengyang City, Hunan Province, China.*

²*INFN – Istituto Nazionale di Fisica Nucleare – Sezione di Bari, Via Orabona 4, 70125 Bari, Italy*

³*School of Mathematics and Physics, University of South China, No. 28, West Changsheng Road, Hengyang City, Hunan Province, China.*

Uncovering physical laws from experimental data is a fundamental goal of theoretical physics. In this work, we apply the spline-based, interpretable Kolmogorov–Arnold Network (KAN) to explore the algebraic structure underlying the baryon octet and decuplet mass spectra. Within a symbolic regression framework and without imposing theoretical priors, KAN autonomously recovers the classical Gell-Mann–Okubo mass relations and accurately extracts the associated $SU(3)$ symmetry-breaking parameters. Compared to conventional fitting approaches, this method achieves comparable predictive accuracy while offering substantially improved interpretability and analytic transparency. Our results demonstrate the potential of KAN as a powerful tool for symbolic discovery in hadron physics and for bridging data-driven modeling with fundamental physical laws.

Introduction: Within the Standard Model, hadrons—composite particles made of quarks bound by the strong interaction—are described by Quantum ChromoDynamics (QCD). As a non-Abelian gauge theory, QCD successfully accounts for phenomena such as color confinement and asymptotic freedom [1–9], yet its non-perturbative regime, which dominates the hadron spectrum, remains analytically challenging. Even so, the hadron mass spectrum exhibits patterns that reflect the underlying $SU(3)$ flavor symmetry [10–12]. In the 1960s, Gell-Mann and Ne’eman introduced the Eightfold Way classification, organizing the rapidly expanding set of experimentally discovered hadrons into octets and decuplets according to symmetry principles [10–12]. This framework indirectly led to the quark model, in which baryons and mesons are understood as three-quark states and quark–antiquark pairs, respectively. The first observation of the exotic candidate $X(3872)$ in 2003 challenged this simple three-quark picture. Since then, numerous exotic candidates have been reported at major high-energy accelerators [13–22], motivating efforts to develop more general mass formulas capable of describing these new states and predicting future ones. Within a single $SU(3)$ multiplet, small mass splittings arise from differences in the up, down, and strange quark masses. To quantify this effect, Gell-Mann and Okubo proposed the well-known GMO mass formula [12], which serves both as a valuable phenomenological tool and as a benchmark for testing flavor-symmetry breaking effects.

In recent years, machine learning (ML) has made significant advances across a wide range of disciplines. In physics, ML has been used to explore theoretical frameworks [23] and to analyze high-energy phenomena [24–37]. Machine learning (ML) techniques enable the extraction of physical information from high-dimensional

data—tasks that are often difficult to accomplish using traditional methods. Neural networks, in particular, excel at approximating nonlinear mappings and uncovering hidden patterns in both experimental and simulated data. In addition, physics-informed neural networks (PINNs) [38, 39] and their extensions embed physical constraints directly into the learning process, thereby bridging the gap between data-driven models and theoretical frameworks.

Among emerging neural network architectures, the Kolmogorov–Arnold Network (KAN) [40, 41] stands out for its interpretability and symbolic regression capabilities. Inspired by the Kolmogorov–Arnold representation theorem, KAN replaces the fixed weights of conventional neural networks with learnable univariate functions, enabling it to represent complex multivariate relationships in a form that is both flexible and analytically tractable. By expressing learned relations in explicit symbolic form, KAN explicitly addresses the black-box limitation of conventional neural networks and enables transparent physical interpretation. Unlike traditional neural networks [42], symbolic regression methods [43, 44], or genetic algorithms [45], KAN combines the expressive power of neural networks with the interpretability of symbolic regression, while offering higher sample efficiency and better integration of physical priors. Applications of KAN in physics are steadily expanding; for example, it has been used to model and compute the heavy-quark potential via holographic methods combined with lattice QCD data [46]. Such successes highlight KAN’s considerable potential for tackling complex scientific problems [46–49].

In this study, we employ a KAN-based symbolic regression approach to analyze baryon mass data from $SU(3)$ octets and decuplets. Our objectives are: (i) to recover the Gell-Mann–Okubo (GMO) formula [10–12] using modern data-driven techniques; (ii) to assess its generalization capability across different $SU(3)$ multiplets; and (iii) to demonstrate how KAN can bridge machine learning and interpretable physics. Notably, we not only

* chenxun@usc.edu.cn

† xyzhu0128@163.com

‡ wenluo-ok@163.com

successfully reconstruct the classical GMO formula [10–12] but also uncover hidden relationships among quantum numbers within the octet and decuplet, offering new perspectives on flavor-symmetry breaking.

Framework: In the section, we will introduce the detailed training progress. The fundamental structure is presented below:

1. *Input data:* In this study, we use the baryon masses of the SU(3) octet and decuplet as the primary input data. To alleviate the limitations imposed by the small sample size, we employ a physics-motivated perturbative data-augmentation strategy. Specifically, by fixing the relevant group-theoretical quantum numbers — such as isospin (I) and hypercharge (Y) — we introduce controlled variations to the baryon masses (M) within their experimental uncertainties, thereby generating additional samples that remain consistent with SU(3) symmetry. The mass values are taken from the Particle Data Group (PDG) in Table I [50]. For each baryon, multiple perturbed samples are drawn from the corresponding uncertainty interval, resulting in augmented datasets consisting of 1000 samples each for the octet and decuplet. This procedure preserves the underlying symmetry structure while allowing the KAN neural network [40, 41] to effectively learn intrinsic mass-distribution patterns, providing high-quality input for symbolic regression.

Based on this dataset, we apply KAN for symbolic regression to explore hidden relationships between baryon masses and quantum numbers. In the decuplet analysis, KAN autonomously identifies the simplest mathematical expression consistent with both the data and the symmetry constraints, revealing a clear linear dependence of baryon masses on quantum numbers—fully consistent with the expected equal-spacing behavior. This data-driven discovery not only validates the effectiveness of SU(3) flavor symmetry but also demonstrates that the KAN model can recover fundamental linear relations from experimental data without prior assumptions. Building on this linear pattern, we further perform symbolic regression to reconstruct the explicit functional form of the decuplet Gell-Mann–Okubo formula.

For the octet analysis, we adopt the same preprocessing and stratified sampling procedures as in the decuplet case, applying KAN symbolic regression to investigate the quadratic relationship between hypercharge(Y) and isospin(I). The model extracts a compact and physically interpretable expression that accurately captures the observed dependence of octet baryon masses on Y and I . This relation serves as the foundation for fitting the complete Gell-Mann–Okubo formula, which is successfully recovered through further symbolic regression.

The final symbolic expressions obtained for both the octet and decuplet exhibit high accuracy and interpretability, and remain fully consistent with theoretical expectations of SU(3) flavor-symmetry breaking [10–12].

2. *Model Selection:* To ensure that the symbolic regression model is both physically interpretable and capable of accurately capturing the SU(3) baryon mass patterns,

we implemented a systematic model-selection process.

Initially, a custom-parameterized model was trained and evaluated, followed by iterative adjustments of the training parameters to improve accuracy. Simultaneously, model pruning was performed based on structural visualizations to remove redundant components and enhance efficiency. The refined model was then retrained, and this cycle of tuning and pruning continued until the evaluation metrics met the desired threshold.

Upon achieving satisfactory performance, symbolic regression [44] was applied. Constrained by the Physics Filter, the regression avoided overly complex functional forms, yielding a physically interpretable expression:

$$f(Y, I) = a Y + b \left[I(I + 1) - \frac{1}{4} Y^2 \right] + c. \quad (1)$$

where a , b , and c are free parameters determined from the data.

3. *SU(3)-consistent generalization:* We assess generalization in the sense of SU(3) multiplet consistency, both at the level of symbolic structure and representation-wide coverage. For the model, a nontrivial requirement is that a single invariant symbolic form be shared by all members of a given multiplet—for instance, the KAN-based regression of the Gell–Mann–Okubo relation for octet baryons retains a consistent functional structure across all multiplet members. For the data, the model must perform reliably for all baryons within a given SU(3) representation. The separately trained decuplet model, for example, fits all members from Δ to Ω while naturally reproducing the expected equal-spacing pattern characteristic of the decuplet.

4. *Loss function:* Model performance is evaluated using the mean squared error [51–56] (MSE), defined as

$$\text{MSE} = \frac{1}{n} \sum_{i=1}^n (\hat{y}_i - y_i)^2. \quad (2)$$

This metric measures the average squared deviation between predictions and observations. During training, numerical gradient descent with a chosen learning rate minimizes the MSE, optimizing model parameters for accuracy. In symbolic regression [44], optimization extends beyond parameter fitting to include structural discovery. Thus, MSE not only quantifies prediction error but also facilitates the joint evolution of model structure and parameter convergence.

5. *Training progress of decuplet baryons:* Regarding the decuplet baryons, To explore possible latent linear patterns among the SU(3) decuplet baryons, we applied a KAN-based symbolic regression to their experimental mass data. Rather than prescribing a predefined functional form, the network autonomously searched for the simplest mathematical expression consistent with the data and symmetry constraints. After training, the resulting symbolic form revealed a clear linear dependence between baryon masses and their quantum numbers, consistent with the expected equal-spacing behavior within the decuplet.

TABLE I. Baryon multiplet properties under SU(3) flavor symmetry. Masses (in MeV/c^2) represent isospin-averaged values from PDG database [50], with uncertainties spanning the full range of observed states within each multiplet. Decuplet states ($J^P = 3/2^+$) and octet states ($J^P = 1/2^+$) are distinguished by their spin-parity quantum numbers and quark composition.

Name	Symbol	I	Y	Mass (MeV/ c^2)
Octet				
Nucleons	N	$\frac{1}{2}$	1	939 ± 1
Lambda baryons	Λ	0	0	1116 ± 1
Sigma baryons	Σ	1	0	1193 ± 4
Xi baryons	Ξ	$\frac{1}{2}$	-1	1318 ± 3
Decuplet				
Delta baryons	Δ	$\frac{3}{2}$	1	1232 ± 2
Sigma baryons	Σ^*	1	0	1385 ± 3
Xi baryons	Ξ^*	$\frac{1}{2}$	-1	1533 ± 2
Omega baryon	Ω	0	-2	1672 ± 1

This data-driven discovery not only reaffirms the validity of the SU(3) flavor symmetry but also demonstrates the ability of the KAN model to recover fundamental linear relations directly from empirical data without prior assumptions. The extracted formula provides a quantitative bridge between the group-theoretic structure of the decuplet and the experimentally observed mass spectrum.

This figure 1 illustrates the KAN neural network architecture employed to investigate the linear relations in the decuplet, which consists of two hidden layers. As shown in Table II, the final results were obtained after two rounds of training and pruning. Beyond these two iterations, further training produced no change in the loss function, indicating that the model had converged. The final formula obtained for decuplet baryons is:

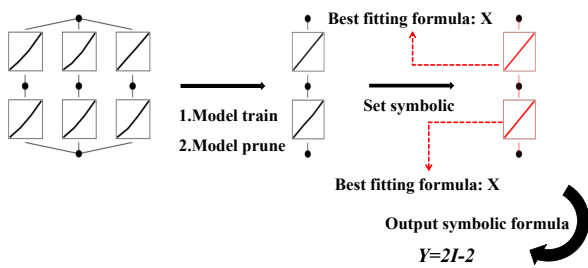


FIG. 1. This figure illustrates the process of using a KAN neural network to uncover linear relationships among decuplet baryons.

$$Y_{10} = 2I_{10} - 2. \quad (3)$$

Building on the identified linear patterns within the SU(3) decuplet, we performed symbolic regression to re-

TABLE II. training log of decuplet linear

Step	train loss	test loss
1	4.05×10^{-2}	4.29×10^{-2}
2	3.25×10^{-10}	1.73×10^{-10}

cover the explicit functional dependence between baryon masses and their quantum numbers. Using experimental data from PDG [50], the KAN model was trained to learn this mapping in a data-driven yet physically constrained manner. The regression converged rapidly with low loss, indicating that the network effectively captured the underlying symmetry structure.

Further, to obtain the GMO formula for the decuplet, we constructed a KAN with a (2,3,1) architecture, corresponding to the number of nodes in the input, hidden, and output layers, respectively, as shown in figure 2. The input variables are hypercharge Y and isospin I , and the output is the mass M . During training, the regularization parameters and learning rate were adjusted adaptively after each iteration to reduce the loss to an appropriate level. At the same time, the model automatically identified and removed redundant or ineffective branches, thereby improving generalization and reducing computational complexity. Through pruning, the network structure was simplified, retaining only the paths that contributed to the final symbolic regression. After ten training iterations, as shown in Table III, the loss function exhibited no further change, indicating that the model had converged.

The analytical expression obtained from symbolic regression is:

$$F(x_1, x_2) = -871.53(-0.1x_1 - 1)^2 + 0.05(x_1 + 1)^2 + 22.04(-x_2 - 0.24)^2 - 2.81(-0.7x_2 - 1)^2 + 2231.5. \quad (4)$$

Split the arithmetic expression in the parentheses, and After splitting and retaining two decimal places, the expression becomes:

$$F(x_1, x_2) = -8.67x_1^2 - 174.21x_1 + 20.66x_2^2 + 6.65x_2 + 1358.48. \quad (5)$$

According to the constraints of the GMO formula, combining with the relation $Y_{10} = 2I_{10} - 2$, we proceed to simplify the expression step-by-step to approximate the target form. The detailed derivation is as follows: First, let $x_1 = Y_{10}$ and $x_2 = I_{10}$, and substitute it into the equation and rearrange each term:

$$F(Y_{10}, I_{10}) = 20.66I_{10}^2 + 20.66I_{10} - 14.01I_{10} - 8.67Y_{10}^2 - 174.21Y_{10} + 1358.48. \quad (6)$$

Next, extract the common factor $Y_{10}(Y_{10} + 1)$ from the Y_{10} -related terms and adjust the remaining components:

$$F(Y_{10}, I_{10}) = 20.66I_{10}(I_{10} + 1) - 181.215Y_{10} - 8.67Y_{10}^2 + 1344.47. \quad (7)$$

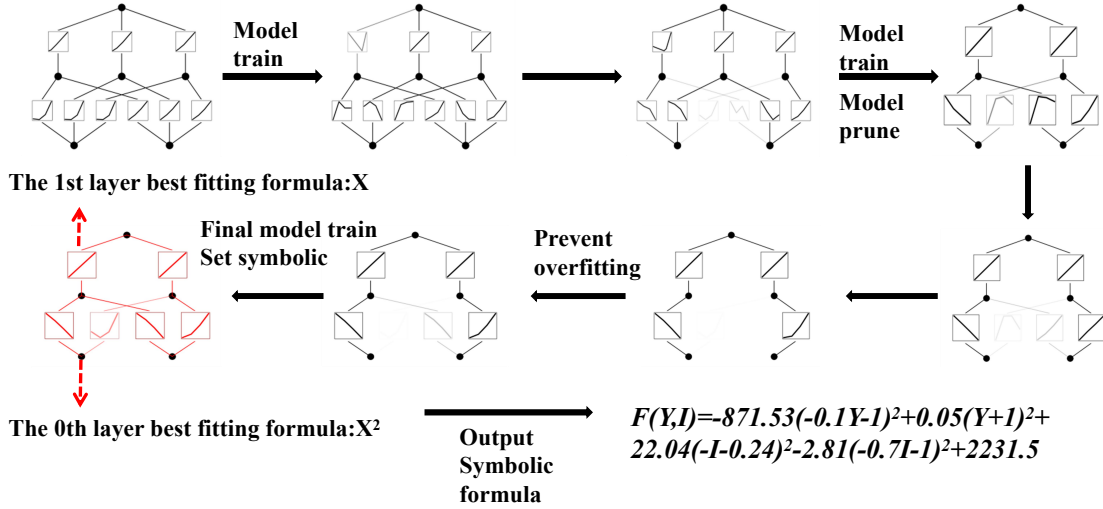


FIG. 2. This figure illustrates the key process of using a KAN neural network to discover the Gell-Mann-Okubo formula for decuplet baryons. including only the essential steps such as key training, pruning, and symbolic regression.

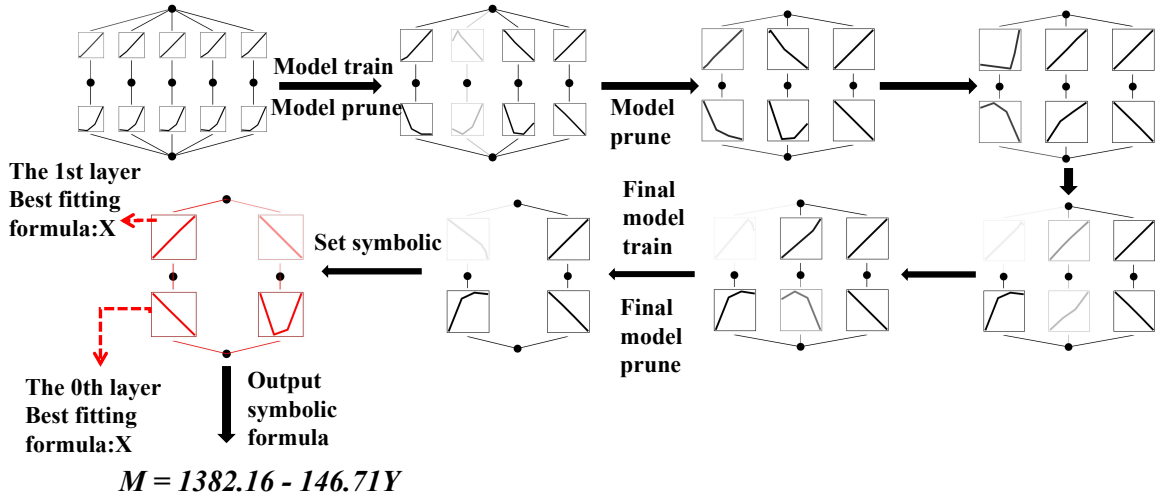


FIG. 3. This figure illustrates the core process of using a KAN neural network to discover the equal spacing rule among decuplet baryons, including only the essential steps such as key training, pruning, and symbolic regression.

To achieve a more compact expression, adjust the coefficients of terms involving Y_{10} and $I_{10}(I_{10} + 1)$:

$$\begin{aligned}
 F(Y_{10}, I_{10}) &= -90.5Y_{10}^2 - 672.27Y_{10} + 689.73 \\
 &\quad + 348.03I_{10}(I_{10} + 1). \\
 &= -253.5Y_{10}^2 - 1650.27Y_{10} - 614.27 \\
 &\quad + 1000.03I_{10}(I_{10} + 1).
 \end{aligned} \tag{8}$$

To obtain a form similar to Eq. (1), and taking into account the constraint $Y_{10} = 2I_{10} - 2$, we can simplify the above expression to the following form:

$$\begin{aligned}
 M_{10} &= -5550.27Y_{10} - 903.5Y_{10}^2 \\
 &\quad + 3600.03I_{10}(I_{10} + 1) - 5814.27.
 \end{aligned} \tag{9}$$

This result not only validates the physical interpretability of the KAN-based regression but also highlights its potential as a tool for uncovering the underlying physical patterns encoded in the data.

TABLE III. Training log of the decuplet GMO.

Step	train loss	test loss
1	1.11×10^{-3}	1.15×10^{-3}
2	1.30×10^{-3}	1.27×10^{-3}
3	1.51×10^{-3}	1.61×10^{-3}
4	1.65×10^{-2}	1.73×10^{-2}
5	2.52×10^{-2}	2.37×10^{-2}
6	7.60×10^{-4}	7.28×10^{-4}
7	5.02×10^{-4}	4.78×10^{-4}
8	4.37×10^{-3}	4.20×10^{-3}
9	4.02×10^{-4}	3.75×10^{-4}
10	9.90×10^{-4}	9.80×10^{-4}

The equal-spacing rule is a remarkably simple yet striking consequence of the GMO mass formula for the baryon decuplet. It states that within the decuplet, each decrease of one unit in strangeness S (corresponding to the addition of a strange quark s) leads to an approximately constant increase in the particle's mass. We can verify this with experimental data:

1. The mass difference from Δ ($S=0$) to Σ^* ($S=-1$):

$$M(\Sigma^*) - M(\Delta) \approx 1385 - 1232 = 153 \text{ MeV}/c^2.$$

2. The mass difference from Σ^* ($S=-1$) to Ξ^* ($S=-2$):

$$M(\Xi^*) - M(\Sigma^*) \approx 1533 - 1385 = 148 \text{ MeV}/c^2.$$

3. The mass difference from Ξ^* ($S=-2$) to Ω^- ($S=-3$):

$$M(\Omega^-) - M(\Xi^*) \approx 1672 - 1533 = 139 \text{ MeV}/c^2.$$

As can be seen, these three mass differences are very close, all around $140 - 150 \text{ MeV}/c^2$. This linear, equally spaced mass relationship is the equal spacing rule of the decuplet. Consequently, the GMO formula reduces to a linear relation,

$$M = M_0 + aY. \quad (10)$$

Here, M is the baryon mass, and M_0 and a are constants parametrizing the SU(3) symmetric contribution and its leading symmetry breaking, respectively. Similarly, we use KAN to train the data in Table I [50] to validate the equal-spacing rule [10–12] in the baryon decuplet. We perform symbolic regression directly on the data to test whether a linear relation between baryon mass M and hypercharge Y can be recovered. The procedure mirrors the previous setup, with minor adjustments to target linearity: the model is initialized with a single-node input layer, a five-node hidden layer, and a single-node output layer. The overall training follows the same workflow, but we impose stricter accuracy requirements and therefore conduct multiple training rounds. The detailed procedure is illustrated in the figure 3. After 10 training iterations, as illustrated in Table IV, the

model approached convergence and symbolic regression was performed, yielding the following expression:

$$M_{10} = 1382.16 - 146.71Y_{10}. \quad (11)$$

After calculation, the root mean square error (RMSE) is approximately 3.530, and the coefficient of determination R^2 is approximately 0.99954. Simultaneously, we observe the spontaneous emergence of a “dominant–correction” hierarchy. Through additive composition, the model effectively decouples the fitting task: smooth activation functions (right) capture the leading-order physical dependence, whereas irregular ones (left) act as numerical residual compensators for local fluctuations. Although these perturbative terms lack intuitive symbolic forms, they are essential for maintaining high regression accuracy by offsetting minor errors. This synergistic mechanism demonstrates KAN's ability to adaptively balance sparse physical representation with numerical precision.

TABLE IV. training log of The equal-spacing rule for the baryon decuplet

Step	train loss	test loss
1	6.43×10^{-3}	6.26×10^{-3}
2	8.09×10^{-3}	7.60×10^{-3}
3	2.34×10^{-3}	2.46×10^{-3}
4	1.08×10^{-3}	9.93×10^{-4}
5	5.04×10^{-4}	4.74×10^{-4}
6	2.09×10^{-3}	2.03×10^{-3}
7	8.73×10^{-4}	8.03×10^{-4}
8	6.57×10^{-4}	5.95×10^{-4}
9	6.92×10^{-4}	7.10×10^{-4}
10	1.85×10^{-4}	1.87×10^{-4}

6. *Training progress of octet baryons:* For the octet baryons, in order to uncover their hidden nonlinear interrelationships, we conducted a second-stage analysis using the same preprocessing and stratified sampling procedures as in the decuplet case, applied to the SU(3) octet data. Through the KAN symbolic regression workflow, we focus on the relationship between hypercharge Y and isospin I among the octet members. Figure 4 illustrates the KAN architecture employed for this task, which is identical to that used in deriving the linear relation for the decuplet, although the training procedure and the function fitting differ. As shown in Table V, the model converged after five training iterations. Finally, symbolic regression was applied to the model, yielding the the relationship between Y and I .

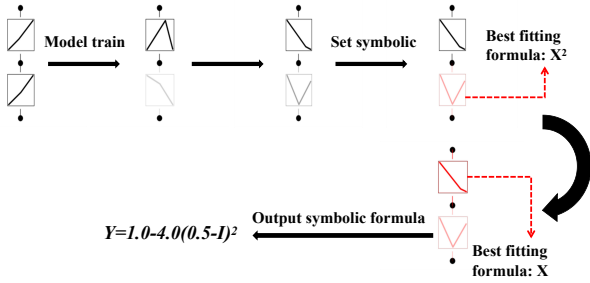


FIG. 4. This figure illustrates the process of using a KAN neural network to uncover binary relationships among octet baryons.

$$Y_8^2 = 1.0 - 4.0(0.5 - I_8)^2. \quad (12)$$

TABLE V. training log of octet binary

Step	train loss	test loss
1	5.35×10^{-2}	5.35×10^{-2}
2	8.09×10^{-2}	8.04×10^{-2}
3	9.67×10^{-2}	1.02×10^{-1}
4	0.00	0.00

Then, we proceed to employ KAN to search for the GMO formula of the octet. The initial neural network architecture was identical to that used for the decuplet, but the parameter adjustments during training differed from the previous setup, with the detailed procedure shown in figure 5. After eight training iterations, the loss function exhibited no further change, and the model was therefore considered converged, as summarized in Table VI. The figure retains only the key stages of training—such as pruning, and optimization. Finally, symbolic regression was applied to the model, yielding the initial expression of the octet GMO formula:

$$F(x_1, x_2) = 355.79(0.39 - x_2)^2 + 142.62(1 - 0.66x_1)^2 + 918.76. \quad (13)$$

After splitting and retaining two decimal places, simultaneously, replace x_1 with Y_8 and x_2 with I_8 . the initial expression is obtained:

$$F(Y_8, I_8) = 62.13Y_8^2 + 355.79I_8^2 - 188.26Y_8 - 277.52I_8 + 1115.50. \quad (14)$$

To align the coefficients of I_8^2 and I_8 , combine the expression above, and temporarily substitute Y_8^2 for $0.25Y_8^2$ (i.e., the relation $0.25Y_8^2 = I_8 - I_8^2$).

The I_8 -related terms can be integrated into the original

expression through the following transformation:

$$\begin{aligned} & 39.135I_8 + 39.135I_8^2 - 39.135I_8 \\ & - 39.135I_8^2 - 277.52I_8 + 355.79I_8^2 \\ & = 39.135I_8(I_8 + 1) - 316.655I_8 + 316.655I_8^2 \\ & = 39.135I_8(I_8 + 1) - 316.655I_8(1 - I_8) \\ & = 39.135I_8(I_8 + 1) - 316.655 \cdot 0.25Y_8^2 \\ & = 39.135I_8(I_8 + 1) - 79.16375Y_8^2. \end{aligned} \quad (15)$$

Substitute the above result into the original expression and consolidate all coefficients to obtain the form:

$$\begin{aligned} F(Y_8, I_8) &= 39.135I_8(I_8 + 1) - 79.16375Y_8^2 - 188.26Y_8 \\ &+ 62.13Y_8^2 + 1115.50 \\ &= 39.14I_8(I_8 + 1) - 17.03Y_8^2 - \\ &188.26Y_8 + 1115.50. \end{aligned} \quad (16)$$

Finally, replace $F(Y_8, I_8)$ with M_8 to obtain the final form:

$$\begin{aligned} M_8 &= -188.26Y_8 + 39.14I_8(I_8 + 1) \\ &- 17.03Y_8^2 + 1115.50. \end{aligned} \quad (17)$$

TABLE VI. training log of octet GMO

Step	train loss	test loss
1	1.27×10^{-2}	1.29×10^{-2}
2	4.60×10^{-3}	4.60×10^{-3}
3	7.87×10^{-4}	7.85×10^{-4}
4	8.79×10^{-3}	8.81×10^{-3}
5	4.04×10^{-3}	4.05×10^{-3}
6	3.64×10^{-9}	1.37×10^{-9}
7	5.19×10^{-8}	5.32×10^{-10}
8	2.92×10^{-11}	9.99×10^{-13}

7. *Output:* For the SU(3) decuplet baryons (as shown in the decuplet section of Table VII), KAN-based symbolic regression first identifies a linear dependence between Y and I , which is then incorporated into the GMO expression. After algebraic simplification, the complete decuplet GMO relation is obtained, naturally containing the equal-spacing rule and showing excellent agreement with experimental results.

For the SU(3) octet baryons (as shown in the octet section of Table VII), the method reveals a multivariate correlation between Y and I . Substituting this relation into the symbolic GMO expression yields a compact and interpretable octet GMO formula, consistent with the empirical mass hierarchy.

Conclusion and outlook: In this work, we employ KAN to perform symbolic regression on experimental baryon mass data from SU(3) octets and decuplets, with the dual aims of rediscovering the GMO mass formulas and refining their functional forms directly from data. Given

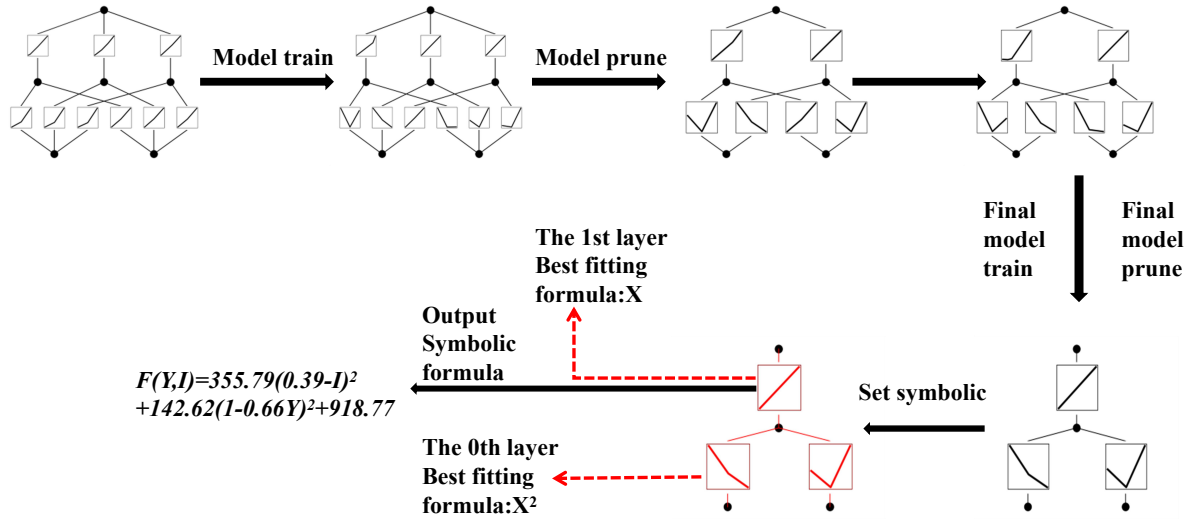


FIG. 5. This figure illustrates the process of using a KAN neural network to uncover the Gell-Mann–Okubo formula for octet baryons.

TABLE VII. The table presents all the results for the decuplet and octet baryons obtained in this study using the KAN neural network.

Decuplet
Relation
$Y_{10} = 2I_{10} - 2$
$M_{10} = -5550.27Y_{10} - 903.5Y_{10}^2 + 3600.03I_{10}(I_{10} + 1) - 5814.27$
$M_{10}(\text{equal-spacing}) = 1382.16 - 146.71Y_{10}$

Octet
Relation
$Y_8^2 = 1.0 - 4.0(0.5 - I_8)^2$
$M_8 = -188.26Y_8 + 39.14I_8(I_8 + 1) - 17.03Y_8^2 + 1115.50$

the limited sample size, while preserving SU(3) structure, we use a physically informed, perturbation-based data augmentation procedure that perturbs baryon masses within reported experimental uncertainties while holding group-theoretical quantum numbers (e.g., isospin I and hypercharge Y) fixed; mass values are taken from the PDG and related literatures [10–12, 57, 58]. Model performance, monitored via MSE, guides adaptive tuning of regularization and learning-rate parameters and informs pruning decisions that remove redundant branches and retain only paths relevant for symbolic extraction.

Applying this workflow, KAN consistently extracts compact, physically interpretable symbolic expressions. For the octet, the network uncovers a multivariate relation between Y and I that serves as the basis for recovering the octet GMO formula; the extracted symbolic form generalizes across N , Λ , Σ , and Ξ . For the decuplet, KAN

autonomously finds a simplest-form linear dependence of mass on quantum numbers and, building on that linear pattern, reconstructs an explicit decuplet GMO expression that reproduces the expected equal-spacing rule from Δ to Ω . These invariant symbolic forms capture internal SU(3) flavor-symmetry breaking patterns and outperform purely numerical fits by revealing analytic structure and hidden relations among multiplet quantum numbers.

More broadly, the physical significance of this study lies in demonstrating the possibility of reconstructing underlying physical symmetries directly from experimental observations. Using KAN, we independently identify the SU(3) flavor symmetry governing the hadron mass spectrum, together with its symmetry-breaking patterns, without introducing prior group-theoretical assumptions. This approach provides a model-independent framework for quantitatively characterizing symmetry-breaking effects induced by quark mass differences, and establishes an interpretable, data-driven paradigm for exploring unknown regularities in hadron spectra in regimes where a complete analytic theory is not yet available.

Beyond validating SU(3) expectations, our results demonstrate KAN’s advantage as a data-driven, assumption-light method for rediscovering empirical mass formulas. The approach suggests several promising directions, including applying KAN to more intricate hadron spectra and exotic states [13, 59–63], integrating QCD inputs or expanded experimental datasets [57, 58, 64–80] to further refine symbolic forms, and improving symbolic-regression pipelines to enhance interpretability and predictive power in high-energy physics. Overall, our findings highlight KAN’s potential to bridge data-driven modeling and interpretable physical laws.

ACKNOWLEDGMENTS

This work is supported by the National Natural Science Foundation of China (NSFC) Grant Nos: 12405154, and the European Union – Next Generation EU through the research grant number P2022Z4P4B “SOPHYA -

Sustainable Optimised PHYsics Algorithms: fundamental physics to build an advanced society” under the program PRIN 2022 PNRR of the Italian Ministero dell’Università e Ricerca (MUR).

REFERENCES

- [1] D. J. Gross and F. Wilczek, Ultraviolet behavior of non-abelian gauge theories, *Physical Review Letters* **30**, 1343 (1973).
- [2] H. D. Politzer, Reliable perturbative results for strong interactions?, *Physical Review Letters* **30**, 1346 (1973).
- [3] C. G. Callan Jr, Broken scale invariance in scalar field theory, *Physical Review D* **2**, 1541 (1970).
- [4] K. Symanzik, Small distance behaviour in field theory and power counting, *Communications in Mathematical Physics* **18**, 227 (1970).
- [5] V. Vanyashin and M. Terent’ev, The vacuum polarization of a charged vector field, *Sov. Phys. JETP* **21**, 375 (1965).
- [6] I. Khriplovich, *GREEN’S FUNCTIONS IN THEORIES WITH NON-ABELIAN GAUGE GROUP.*, Tech. Rep. (Inst. of Nuclear Physics, Novosibirsk, USSR, 1969).
- [7] H. Fritzsch, M. Gell-Mann, and H. Leutwyler, Advantages of the color octet gluon picture, *Physics Letters B* **47**, 365 (1973).
- [8] D. J. Gross and F. Wilczek, Asymptotically free gauge theories. i, *Physical Review D* **8**, 3633 (1973).
- [9] H. D. Politzer, Asymptotic freedom: An approach to strong interactions, *Physics Reports* **14**, 129 (1974).
- [10] M. Gell-Mann, The eightfold way: A theory of strong interaction symmetry, in *The Eightfold Way* (CRC Press, 2018) pp. 11–57.
- [11] S. Okubo, Note on unitary symmetry in strong interactions, *Progress of Theoretical Physics* **27**, 949 (1962).
- [12] M. Gell-Mann, Symmetries of baryons and mesons, in *The eightfold way* (CRC Press, 2018) pp. 216–233.
- [13] H.-X. Chen, W. Chen, X. Liu, and S.-L. Zhu, The hidden-charm pentaquark and tetraquark states, *Physics Reports* **639**, 1 (2016).
- [14] Y.-R. Liu, H.-X. Chen, W. Chen, X. Liu, and S.-L. Zhu, Pentaquark and tetraquark states, *Progress in Particle and Nuclear Physics* **107**, 237 (2019).
- [15] H.-X. Chen, W. Chen, X. Liu, Y.-R. Liu, and S.-L. Zhu, A review of the open charm and open bottom systems, *Reports on Progress in Physics* **80**, 076201 (2017).
- [16] Y. Dong, A. Faessler, and V. E. Lyubovitskij, Description of heavy exotic resonances as molecular states using phenomenological lagrangians, *Progress in Particle and Nuclear Physics* **94**, 282 (2017).
- [17] R. F. Lebed, R. E. Mitchell, and E. S. Swanson, Heavy-quark qcd exotica, *Progress in Particle and Nuclear Physics* **93**, 143 (2017).
- [18] F.-K. Guo, C. Hanhart, U.-G. Meißner, Q. Wang, Q. Zhao, and B.-S. Zou, Hadronic molecules, *Reviews of Modern Physics* **90**, 015004 (2018).
- [19] R. M. Albuquerque, J. M. Dias, K. Khemchandani, A. M. Torres, F. S. Navarra, M. Nielsen, and C. M. Zanetti, Qcd sum rules approach to the x, y and z states, *Journal of Physics G: Nuclear and Particle Physics* **46**, 093002 (2019).
- [20] Y. Yamaguchi, A. Hosaka, S. Takeuchi, and M. Takizawa, Heavy hadronic molecules with pion exchange and quark core couplings: a guide for practitioners, *Journal of Physics G: Nuclear and Particle Physics* **47**, 053001 (2020).
- [21] F.-K. Guo, X.-H. Liu, and S. Sakai, Threshold cusps and triangle singularities in hadronic reactions, *Progress in Particle and Nuclear Physics* **112**, 103757 (2020).
- [22] N. Brambilla, S. Eidelman, C. Hanhart, A. Nefediev, C.-P. Shen, C. E. Thomas, A. Vairo, and C.-Z. Yuan, The xyz states: experimental and theoretical status and perspectives, *Physics reports* **873**, 1 (2020).
- [23] S. J. Wetzel, R. G. Melko, J. Scott, M. Panju, and V. Ganesh, Discovering symmetry invariants and conserved quantities by interpreting siamese neural networks, *Physical Review Research* **2**, 033499 (2020).
- [24] Y. D. Hezaveh, L. P. Levasseur, and P. J. Marshall, Fast automated analysis of strong gravitational lenses with convolutional neural networks, *Nature* **548**, 555 (2017).
- [25] S. Soma, L. Wang, S. Shi, H. Stöcker, and K. Zhou, Reconstructing the neutron star equation of state from observational data via automatic differentiation, *Physical Review D* **107**, 083028 (2023).
- [26] L.-G. Pang, K. Zhou, N. Su, H. Petersen, H. Stöcker, and X.-N. Wang, An equation-of-state-meter of quantum chromodynamics transition from deep learning, *Nature communications* **9**, 210 (2018).
- [27] X. Chen and M. Huang, Machine learning holographic black hole from lattice qcd equation of state, *Physical Review D* **109**, L051902 (2024).
- [28] A. Radovic, M. Williams, D. Rousseau, M. Kagan, D. Bonacorsi, A. Himmel, A. Aurisano, K. Terao, and T. Wongjirad, Machine learning at the energy and intensity frontiers of particle physics, *Nature* **560**, 41 (2018).
- [29] D. Guest, K. Cranmer, and D. Whiteson, Deep learning and its application to lhc physics, *Annual Review of Nuclear and Particle Science* **68**, 161 (2018).
- [30] K. Albertsson, P. Altoe, D. Anderson, M. Andrews, J. P. Araque Espinosa, A. Aurisano, L. Basara, A. Bevan, W. Bhimji, D. Bonacorsi, *et al.*, Machine learning in high energy physics community white paper, in *Journal of Physics: Conference Series*, Vol. 1085 (IOP Publishing, 2018) p. 022008.
- [31] J. Kim, G. Pederiva, and A. Shindler, Machine learning mapping of lattice correlated data, *Physics Letters B* **856**, 138894 (2024).

[32] K. Zhou, L. Wang, L.-G. Pang, and S. Shi, Exploring qcd matter in extreme conditions with machine learning, *Progress in Particle and Nuclear Physics* **135**, 104084 (2024).

[33] G. Aarts, K. Fukushima, T. Hatsuda, A. Ipp, S. Shi, L. Wang, and K. Zhou, Physics-driven learning for inverse problems in quantum chromodynamics, *Nature Reviews Physics* **7**, 154 (2025).

[34] L. Jiang, L. Wang, and K. Zhou, Deep learning stochastic processes with qcd phase transition, *Physical Review D* **103**, 116023 (2021).

[35] X. Chen and M. Huang, Flavor dependent critical endpoint from holographic qcd through machine learning, *Journal of High Energy Physics* **2025**, 1 (2025).

[36] M. Mansouri, K. B. Fadafan, and X. Chen, Holographic complex potential of a quarkonium from deep learning, *arXiv preprint arXiv:2406.06285* (2024).

[37] W.-C. Dai, O.-Y. Luo, B. Chen, X. Chen, X.-Y. Zhu, and X.-H. Li, Extracting transport properties of quark-gluon plasma from the heavy-quark potential with neural networks in a holographic model, *arXiv preprint arXiv:2503.10213* (2025).

[38] M. Raissi, P. Perdikaris, and G. E. Karniadakis, Physics-informed neural networks: A deep learning framework for solving forward and inverse problems involving nonlinear partial differential equations, *Journal of Computational physics* **378**, 686 (2019).

[39] P.-H. Chiu, J. C. Wong, C. Ooi, M. H. Dao, and Y.-S. Ong, Can-pinn: A fast physics-informed neural network based on coupled-automatic-numerical differentiation method, *Computer Methods in Applied Mechanics and Engineering* **395**, 114909 (2022).

[40] Z. Liu, Y. Wang, S. Vaidya, F. Ruehle, J. Halverson, M. Soljačić, T. Y. Hou, and M. Tegmark, Kan: Kolmogorov-arnold networks, *arXiv preprint arXiv:2404.19756* (2024).

[41] Z. Liu, P. Ma, Y. Wang, W. Matusik, and M. Tegmark, Kan 2.0: Kolmogorov-arnold networks meet science, *arXiv preprint arXiv:2408.10205* (2024).

[42] Z. Liu and M. Tegmark, Machine learning conservation laws from trajectories, *Physical Review Letters* **126**, 180604 (2021).

[43] S.-M. Udrescu and M. Tegmark, Ai feynman: A physics-inspired method for symbolic regression, *Science advances* **6**, eaay2631 (2020).

[44] M. Schmidt and H. Lipson, Distilling free-form natural laws from experimental data, *science* **324**, 81 (2009).

[45] Z. Zhang, R. Ma, J. Hu, and Q. Wang, Approach the gell-mann-okubo formula with machine learning, *Chinese Physics Letters* **39**, 111201 (2022).

[46] O.-Y. Luo, X. Chen, F.-P. Li, X.-H. Li, and K. Zhou, Neural network modeling of heavy-quark potential from holography, *The European Physical Journal C* **85**, 637 (2025).

[47] N. R. Panczyk, O. F. Erdem, and M. I. Radaideh, Opening the black-box: Symbolic regression with kolmogorov-arnold networks for energy applications, *arXiv preprint arXiv:2504.03913* (2025).

[48] C. Guo, L. Sun, S. Li, Z. Yuan, and C. Wang, Physics-informed kolmogorov-arnold network with chebyshev polynomials for fluid mechanics, *Physics of Fluids* **37** (2025).

[49] H. Hao, X. Zhang, B. Li, and A. Zhou, A first look at kolmogorov-arnold networks in surrogate-assisted evolutionary algorithms, *arXiv preprint arXiv:2405.16494* (2024).

[50] K. Nakamura, Review of particle physics, *Journal of Physics G: Nuclear and Particle Physics* **37** (2010).

[51] T. Hastie, R. Tibshirani, J. Friedman, *et al.*, *The elements of statistical learning* (2009).

[52] C. M. Bishop, *Pattern recognition and machine learning by Christopher M. Bishop*, Vol. 400 (Springer Science+Business Media, LLC Berlin, Germany:, 2006).

[53] I. Goodfellow, Y. Bengio, A. Courville, and Y. Bengio, *Deep learning*, Vol. 1 (MIT press Cambridge, 2016).

[54] S. Geman, E. Bienenstock, and R. Doursat, Neural networks and the bias/variance dilemma, *Neural computation* **4**, 1 (1992).

[55] K. P. Murphy, *Machine learning: a probabilistic perspective* (MIT press, 2012).

[56] T. Hastie, R. Tibshirani, and J. Friedman, *An introduction to statistical learning*, (2009).

[57] Y.-F. Liu, W.-J. Xing, X.-Y. Wu, G.-Y. Qin, S. Cao, and H. Xing, Heavy and light flavor jet quenching in different collision systems at energies available at the cern large hadron collider, *Physical Review C* **105**, 044904 (2022).

[58] S. Katel, H. Li, Z. Zhao, R. Kansal, F. Mokhtar, and J. Duarte, Learning symmetry-independent jet representations via jet-based joint embedding predictive architecture, *arXiv preprint arXiv:2412.05333* (2024).

[59] H. Garcilazo and A. Valcarce, Exotic heavy hadrons, *Symmetry* **17**, 1324 (2025).

[60] T. Hyodo, Study of hadron interactions and compositeness, *arXiv preprint arXiv:2503.15376* (2025).

[61] G. Yang, J. Ping, and J. Segovia, Tetra-and penta-quark structures in the constituent quark model, *Symmetry* **12**, 1869 (2020).

[62] W.-T. Lyu, L.-J. Liu, and E. Wang, Evidence of the open-flavor tetraquark $t_{c\bar{s}2}$ in the process $b^+ \rightarrow d^{*-}d_s^+\pi^+$, *arXiv preprint arXiv:2501.02839* (2025).

[63] P. D. Collins and E. J. Squires, *Regge poles in particle physics*, Vol. 45 (Springer, 2006).

[64] K. G. Wilson, Confinement of quarks, *Physical review D* **10**, 2445 (1974).

[65] S. Durr, Z. Fodor, J. Frison, C. Hoelbling, R. Hoffmann, S. D. Katz, S. Krieg, T. Kurth, L. Lellouch, T. Lippert, *et al.*, Ab initio determination of light hadron masses, *Science* **322**, 1224 (2008).

[66] Y. Aoki, T. Blum, G. Colangelo, S. Collins, M. D. Morte, P. Dimopoulos, S. Dür, X. Feng, H. Fukaya, M. Golterman, *et al.*, Flag review 2021, *The European Physical Journal C* **82**, 869 (2022).

[67] A. Bazavov, T. Bhattacharya, C. DeTar, H.-T. Ding, S. Gottlieb, R. Gupta, P. Hegde, U. Heller, F. Karsch, E. Laermann, *et al.*, Equation of state in (2+1)-flavor qcd, *Physical Review D* **90**, 094503 (2014).

[68] S. He, L. Li, Z. Li, and S.-J. Wang, Gravitational waves and primordial black hole productions from gluodynamics by holography, *Science China Physics, Mechanics & Astronomy* **67**, 240411 (2024).

[69] L. Zhang and M. Huang, Holographic cold dense matter constrained by neutron stars, *Physical Review D* **106**, 096028 (2022).

[70] Y. Chen, D. Li, and M. Huang, The dynamical holographic qcd method for hadron physics and qcd matter, *Communications in Theoretical Physics* **74**, 097201 (2022).

[71] R. Li, S. Han, Z. Lin, L. Wang, K. Zhou, and S. Shi, Towards constraining qcd phase transitions in neutron star interiors: Bayesian inference with tov linear response analysis, arXiv preprint arXiv:2501.15810 (2025).

[72] K. Zhou, G. Endrődi, L.-G. Pang, and H. Stöcker, Regressive and generative neural networks for scalar field theory, *Physical Review D* **100**, 011501 (2019).

[73] X. Chen, D. Li, and M. Huang, Criticality of qcd in a holographic qcd model with critical end point, *Chinese Physics C* **43**, 023105 (2019).

[74] X. Chen, L. Zhang, D. Li, D. Hou, and M. Huang, Gluodynamics and deconfinement phase transition under rotation from holography, *Journal of High Energy Physics* **2021**, 1 (2021).

[75] X. Chen, D. Li, D. Hou, and M. Huang, Quarkyonic phase from quenched dynamical holographic qcd model, *Journal of High Energy Physics* **2020**, 1 (2020).

[76] L. Zhu, X. Chen, K. Zhou, H. Zhang, and M. Huang, Bayesian inference of the critical end point in a (2+ 1)-flavor system from holographic qcd, *Physical Review D* **112**, 026019 (2025).

[77] W.-J. Xing, S. Cao, G.-Y. Qin, and X.-N. Wang, Flavor hierarchy of jet energy correlators inside the quark-gluon plasma, *Physical Review Letters* **134**, 052301 (2025).

[78] S. Cao and X.-N. Wang, Jet quenching and medium response in high-energy heavy-ion collisions: a review, *Reports on Progress in Physics* **84**, 024301 (2021).

[79] W.-J. Zhang, Z. Zhang, J. Hu, B.-N. Lu, J.-Y. Pang, and Q. Wang, Machine learning unveils the power law of finite-volume energy shifts, *Chinese Physics Letters* (2025).

[80] H.-A. Zeng, L. Wang, and M. Huang, HoloNet: Toward a Unified Einstein-Maxwell-Dilaton Framework of QCD, (2025), [arXiv:2512.06044 \[hep-lat\]](https://arxiv.org/abs/2512.06044).